JGR Space Physics

RESEARCH ARTICLE
10.1029/2023JA031596

Interhemispheric Observations of ULF Waves Caused by Foreshock Transients Under Quiet Solar Wind Conditions

Sung Jun Noh[1,2], Hyomin Kim[2], Dogacan Ozturk[3], Ilya Kuzichev[2], Zhonghua Xu[4], Hui Zhang[5], Andrew Vu[3], Terry Liu[6], James M. Weygand[6], Michael D. Hartinger[7], Xueling Shi[4], Mark Engebretson[8], Andrew Gerrard[2], Eun-Hwa Kim[9], Marc Lessard[10], and Christopher T. Russell[6]

[1]Los Alamos National Laboratory, Los Alamos, NM, USA, [2]New Jersey Institute of Technology, Newark, NJ, USA, [3]University of Alaska Fairbanks, Fairbanks, AK, USA, [4]Virginia Tech, Blacksburg, VA, USA, [5]Shandong University, Weihai, China, [6]University of California, Los Angeles, Los Angeles, CA, USA, [7]Space Science Institute, Boulder, CO, USA, [8]Augsburg University, Minneapolis, MN, USA, [9]Princeton Plasma Physics Laboratory, Princeton University, Princeton, NJ, USA, [10]University of New Hampshire, Durham, NH, USA

Key Points:

- Magnetospheric Multiscale observed a series of foreshock transients near the Earth's bow shock
- Pc1 waves and magnetic impulse events are observed by ground magnetometers in both hemispheres following the foreshock transients
- The difference in observation times between hemispheres implies that Pc1 waves are generated in the off-equatorial region

Supporting Information:

Supporting Information may be found in the online version of this article.

Correspondence to:

S. J. Noh,
sjnoh@lanl.gov

Citation:

Noh, S. J., Kim, H., Ozturk, D., Kuzichev, I., Xu, Z., Zhang, H., et al. (2023). Interhemispheric observations of ULF waves caused by foreshock transients under quiet solar wind conditions. *Journal of Geophysical Research: Space Physics*, *128*, e2023JA031596. https://doi.org/10.1029/2023JA031596

Received 15 APR 2023
Accepted 24 AUG 2023

Author Contributions:

Conceptualization: Sung Jun Noh, Hyomin Kim
Data curation: Michael D. Hartinger, Marc Lessard
Formal analysis: Sung Jun Noh, Dogacan Ozturk
Funding acquisition: Hyomin Kim
Investigation: Sung Jun Noh, Hyomin Kim
Methodology: Sung Jun Noh
Resources: Hyomin Kim, Dogacan Ozturk, Hui Zhang, Andrew Vu, James M. Weygand, Michael D. Hartinger, Andrew Gerrard, Marc Lessard, Christopher T. Russell

Abstract Foreshock transient (FT) events are frequently observed phenomena that are generated by discontinuities in the solar wind. These transient events are known to trigger global-scale magnetic field perturbations (e.g., ULF waves). We report a series of FT events observed by the Magnetospheric Multiscale mission in the upstream bow shock region under quiet solar wind conditions. During the event, ground magnetometers observed significant Pc1 wave activity as well as magnetic impulse events in both hemispheres. Ground Pc1 wave observations show ~8 min time delay (with some time differences) from each FT event which is observed at the bow shock. We also find that the ground Pc1 waves are observed earlier in the northern hemisphere compared to the southern hemisphere. The observation time difference between the hemispheres implies that the source region of the wave is the off-equatorial region.

1. Introduction

Electromagnetic ion cyclotron (EMIC) waves are kinetic scale plasma waves excited by an ion cyclotron instability with a frequency below the local proton gyrofrequency that usually falls into the ULF Pc 1–2 (0.1–5 Hz) frequency band in the Earth's magnetosphere. In the classical resonant wave-particle interaction theory, EMIC waves are generated with left-handed polarization and propagate along the background magnetic field (Anderson et al., 1990, 1996; Fraser & McPherron, 1982; Kennel & Petschek, 1966; Noh et al., 2022). It is widely known that EMIC waves play a key role in the charged particle dynamics in the Earth's magnetosphere, especially for the loss of ring current ions and relativistic electrons (Blum & Breneman, 2020; Capannolo et al., 2019; Cornwall et al., 1970; H. Kim et al., 2021; D.-Y. Lee, 2021; Meredith et al., 2003; Ni et al., 2015; Summers & Thorne, 2003; Thorne & Kennel, 1971; Thorne et al., 2006; X. J. Zhang et al., 2019).

In the Earth's magnetosphere, there are two major drivers for the EMIC wave generation. One is the injected energetic ions during geomagnetic storms and substorms. The supply of energetic source particles from the plasmasheet increases free energy for the ion cyclotron instability and predominantly excites waves in the afternoon side through their westward drift around the Earth (Blum et al., 2015; Clausen et al., 2011; Halford et al., 2010; Jordanova et al., 2008; Jun et al., 2019; Noh et al., 2021; Remya et al., 2018; Usanova et al., 2010, 2012; Yahnin et al., 2021). Another major driver is dayside magnetic field compression due to the enhancement of the solar wind dynamic pressure (Cho et al., 2016, 2017; Engebretson et al., 2018; Keika et al., 2013; Usanova, 2021; Xue et al., 2022). Dayside compression of the magnetic field can introduce betatron acceleration of the particles that makes the particle distribution more anisotropic in the direction perpendicular to the magnetic field ($T_\perp/T_\parallel > 1$). In addition to the perpendicular heating, the off-equatorial minimum B pocket also can make the particle distribution anisotropic. McCollough et al. (2010) suggested that the particle distribution in the off-equatorial minimum B region can be anisotropic enough to excite EMIC waves. There have also been observational reports of the off-equatorially generated EMIC waves (Allen et al., 2015; Liu et al., 2013; Vines et al., 2019).

Hot flow anomalies and foreshock bubbles, two important types of foreshock transient (FT) events, are generated by discontinuities (tangential and rotational) in the solar wind magnetic field (Lin, 1997, 2002; Omidi & Sibeck, 2007; Schwartz et al., 1985; Turner et al., 2013, 2020; H. Zhang et al., 2022). FTs have common features

Software: Sung Jun Noh, Dogacan Ozturk, James M. Weygand
Supervision: Hyomin Kim
Validation: Sung Jun Noh
Visualization: Sung Jun Noh
Writing – original draft: Sung Jun Noh
Writing – review & editing: Sung Jun Noh, Hyomin Kim, Ilya Kuzichev, Zhonghua Xu, Terry Liu, James M. Weygand, Michael D. Hartinger, Xueling Shi, Mark Engebretson, Andrew Gerrard, Eun-Hwa Kim

which are density depletion in their center, temperature enhancement, and decrease of the magnetic field as well as pressure compared to the plasma environment in the solar wind. The effects of FTs on the Earth's magnetosphere are usually considered localized compared to the changes in solar wind dynamic pressure but can be significant (Omidi et al., 2010; Sibeck et al., 1999). Since FTs mainly occur very close to the Earth's bow shock, it is non-trivial to determine whether there is an FT event taking place only with solar wind observations at the L1 point.

It has been known that the FTs are related to and can excite ULF waves in the Earth's magnetosphere (Eastwood et al., 2011; Engebretson et al., 2013; Hartinger et al., 2013; Shi et al., 2021; Sibeck et al., 1999; B. Wang et al., 2020, 2021). Eastwood et al. (2011) reported ground Pc3 wave observations possibly triggered by a hot flow anomaly. They estimated that the time difference between the hot flow anomaly near the bow shock and ground signatures is ∼8 min and it is consistent with the estimated traveling time of the Pc 3 wave from the bow shock to the ground.

In this study, we report a series of FT events observed by the magnetospheric multiscale (MMS) mission and two different but related ground ULF wave observations captured by a high-latitude, interhemispheric ground magnetometer array.

2. Data

The MMS mission consists of four identical satellites that are mainly designed to observe the dayside and nightside reconnection regions (Burch et al., 2016). The orbit of MMS covers from 1 up to 12 R_E with 28° inclination. The Fast Plasma Investigation (FPI, Pollock et al., 2016) provides high cadence plasma measurements that cover ion energies from 10 eV to 30 keV. The sampling rate of the burst mode is 120 ms which allows us to analyze the fine structure of the FT within a few minutes scale. The FPI is used for ion density and temperature. The fluxgate magnetometer (Russell et al., 2016) in the Field suite (Torbert et al., 2016) is used to measure the vector magnetic field.

We use arrays of ground magnetometers installed at high latitudes in both the northern and southern hemispheres to measure signatures that propagated down to the ground (C. R. Clauer et al., 2014; Lanzerotti et al., 1990). Table 1 shows a summary of ground stations used in the present study. Ground stations in the northern hemisphere are longitudinally distributed in similar magnetic latitudes (as well as *L*-values). See also Figure 3 in which star symbols indicate equatorial mapping of ground stations based on IGRF and TS05 magnetic field models (Thébault et al., 2015; Tsyganenko & Sitnov, 2005). Southern hemispheric stations have wider latitude coverage. The PG2 to PG5 stations are latitudinally distributed in a similar magnetic longitude. SPA station is in the latitude between PG3 and 4, but with different longitude. For the DC magnetic field measurements, we use fluxgate magnetometers installed in each station. The DC magnetic field data from STF was not available during the interval of interest. For Pc1 wave observations, higher sensitivity is required since the background magnetic field intensity is strong ($\sim 10^4$ nT), but the wave signatures are relatively weak (a few nT or lower). We use induction coil magnetometers which can measure the AC magnetic field.

Solar wind dynamic pressure and magnetic field data are obtained from the OMNI data set (Papitashvili & King, 2020). We use SuperMAG ring current and substorm aurora electrojet (SME) indices (Newell & Gjerloev, 2011, 2012) as a proxy of geomagnetic storms and substorms, respectively.

3. Foreshock Transient Events and Ground Responses Under Quiet Solar Wind Conditions

3.1. Foreshock Transient Events on 1 December 2017

Foreshock bubbles and hot flow anomalies (referred to as FTs hereafter) have common features such as (a) velocity deflection, (b) temperature enhancement, (c) density reduction, and (d) magnetic field reduction (H. Zhang et al., 2022). Figure 1 shows burst-mode MMS1 observations of ion bulk velocity (first row), ion and electron temperature (second row), proton density (third row), and (fourth row) magnetic field in the GSM coordinate system. We found six FT events from 13:57 to 14:42 UT on 1 December 2017. During this time interval, MMS1 was located in the solar wind upstream of the bow shock (see blue square in Figure 3). The first five events turned out to be foreshock bubbles and the last event is a hot flow anomaly. Differentiating foreshock bubbles and hot

Table 1
Information of the Ground Magnetometer Stations Used in This Study

Station	Location			Sampling rate (fluxgate/search-coil)	Organization (fluxgate/search-coil)
	Geo. Lat. (Mag. Lat.)	Geo. Lon. (Mag. Lon.)	L-value (IGRF + TS05)		
Iqaluit (IQA)	63.45°N (70.78°N)	68.31°W (15.20°E)	8.76	1 Hz/10 Hz	NRCan/UNH
Sondrestrom (STF)	66.59°N (71.17°N)	50.57°W (39.06°E)	8.85	1 Hz/10 Hz	DTU/UNH
PG2	84.42°S (75.41°S)	57.96°E (39.41°E)	9.94	1 Hz/10 Hz	VT/UNH
PG3	84.81°S (73.69°S)	37.63°E (36.84°E)	9.53	1 Hz/10 Hz	VT/UNH
PG4	83.34°S (70.96°S)	12.25°E (36.50°E)	8.59	1 Hz/10 Hz	VT/UNH
PG5	81.96°S (69.57°S)	5.71°E (37.35°E)	8.02	1 Hz/10 Hz	VT/UNH
South Pole (SPA)	90.00°S (74.32°S)	N/A (19.02)	9.91	1 Hz/10 Hz	NJIT/UNH

Note. Each station provides both fluxgate and search-coil magnetometer data.

flow anomalies can be achieved by the edges of their shock. Foreshock transients are usually observed with a shock only in their trailing edge. On the other hand, hot flow anomalies have shocks in both leading and trailing edges (Omidi et al., 2010; Turner et al., 2013). For events 1–5, there is only one shock boundary (trailing edge) right after the core region where density and magnetic field show dips. The core can be more easily found from the anti-correlated behavior between temperature (increase) and density (decrease). The dip is less clear for event 4 but the trailing shock is still clear (~14:23:15). In contrast, event 6 shows both leading and trailing shocks before and after the core. All 6 events show clear velocity deflections (top panels). However, both foreshock bubbles and hot flow anomalies are known to play a similar role in the Earth's magnetosheath and magnetopause with depletion of the pressure in the magnetosheath followed by inward and outward motion of the magnetopause (Archer et al., 2014, 2015; Omidi et al., 2016; C.-P. Wang et al., 2021; H. Zhang et al., 2022).

Figure 2 shows the solar wind and geomagnetic conditions from 12 to 17:00 UT. The SuperMAG auroral electrojet index indicates that there was a certain level of auroral electrojet activity (~200 nT) but severe substorms are not expected as the index did not change significantly during the events. The ring current index was mostly close to 0 nT which indicates there was no ring current enhancement, therefore no storm was present during the event. With relatively quiet substorm and geomagnetic storm activity, it is hard to expect that injected energetic ions can trigger significant disturbances that can cause strong wave activity, especially in the dayside magnetosphere. The solar wind dynamic pressure remained at the quiet level (~2 nPa) and did not show considerable enhancement during the event. The solar wind magnetic field pointed southward at the beginning of the events but was mostly close to 0 nT before and during the event interval. This small fluctuation in Bz maintained from before the event could supply particles into the inner magnetosphere to maintain the SME index to a certain level. However, the overall solar wind and geomagnetic conditions were not in a favorable condition to cause strong magnetic disturbances in the outer dayside magnetosphere.

3.2. Ground Observations

Under the relatively quiet solar wind and geomagnetic conditions with a series of FT events shown in Section 3.1, the high-latitude ground magnetometer network observed strong Pc1 wave activity in both the northern and southern hemispheres. Figure 4 shows spectrograms of the AC magnetic field measured by induction coil magnetometers and the two average-subtracted horizontal components of the DC magnetic field measured by fluxgate magnetometers. The top two stations (IQA and STF) are the northern hemispheric stations and the other five stations (PG 2, 3, 4, 5, and SPA) are the southern hemispheric stations. Note that the STF station is located at a latitude between the PG3 and PG4 stations in magnetic coordinates, with a closer L value to PG4, (see Figure 3 and Table 1) based on the IGRF + TS05 model. In both hemispheres, strong and well-defined wave activity is observed during the event interval. Vertical magenta lines in each panel indicate the onset times of FTs observed by MMS1. Orange lines are 8 min after the FT events. The spectrograms show that wave activity is observed ~8 min after FT events, especially for events 1, 4, 5, and 6. This indicates that the 8-min time delay is related to the energy transfer time between the FTs and ground stations in the form of the Pc1 waves. Note that the ground Pc1 waves are not always observed exactly 8 min after each FT event but there are 1–2 min deviations in addition

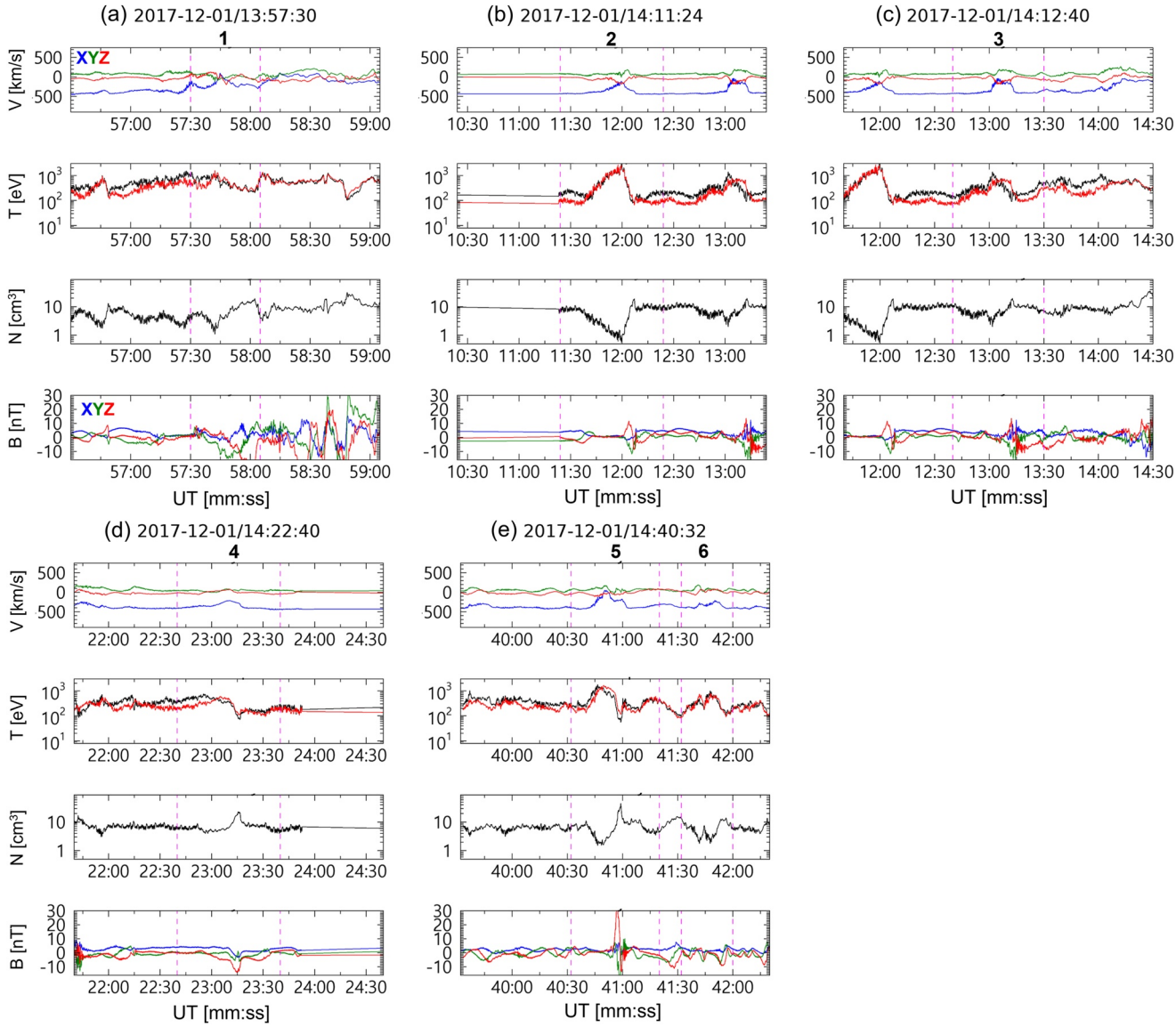

Figure 1. MMS1 observations of the ion bulk velocity (x in blue, y in green, and z in red) in GSM coordinates (first row), proton temperature in perpendicular (red) and parallel (black) directions (second row), proton density (third row), and magnetic field in GSM coordinates (fourth row) for five selected time intervals (a–e) that contain six foreshock transient (FT) events. The numbers at the top of each figure indicate the event number of the FTs. Dashed vertical magenta lines in each plot indicate the start and end time of FT events.

to the 8-min. For example, ground responses related to event 1 occurred slightly later than 8 min but event 4 related waves were observed slightly earlier than 8 min.

The Pc1 wave activity was stronger in the PG2 station where the L value was the highest among the stations and the closest station to the magnetopause (Figure 3). Stronger activity in the outer L stations (with the maximum wave amplitude of 0.16 nT at 14:11 in PG2) and weaker activity for the inner L stations (with the maximum wave amplitude of ~0.020 nT at 14:11 in PG5) implies that the source of the wave was located close to the magnetopause and their activity was radially localized since Pc1 waves are generally known to propagate parallel to the background magnetic field. The typical spatial scale of EMIC waves is known to be about 1 R_E in the magnetosphere (Blum et al., 2017; J. Lee et al., 2013). This could be evidence of wave energy transport from outside of the magnetosphere. The IQA station in the northern hemisphere and the SPA station in the southern hemisphere show less clear and weaker wave activity compared to other stations that are closer to MMS 1. This is because IQA and SPA are longitudinally distant from other stations. The magnetic local time differences between MMS

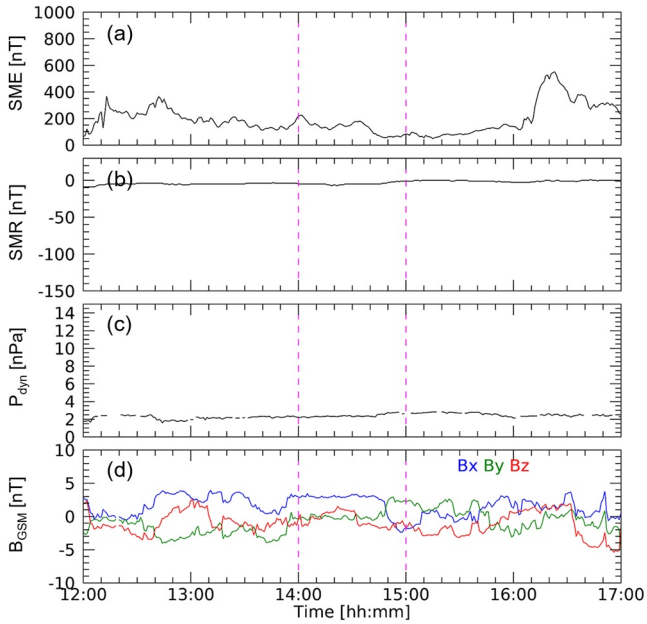

Figure 2. (a) SuperMAG auroral electrojet index (substorm aurora electrojet), (b) SuperMAG ring current (SMR) index, (c) solar wind dynamic pressure, and (d) solar wind magnetic field in GSM coordinates. Vertical magenta lines in each panel indicate 14:00–15:00 UT when the foreshock transient events were observed by MMS1. The solar wind dynamic pressure and magnetic field data were obtained from OMNIWeb.

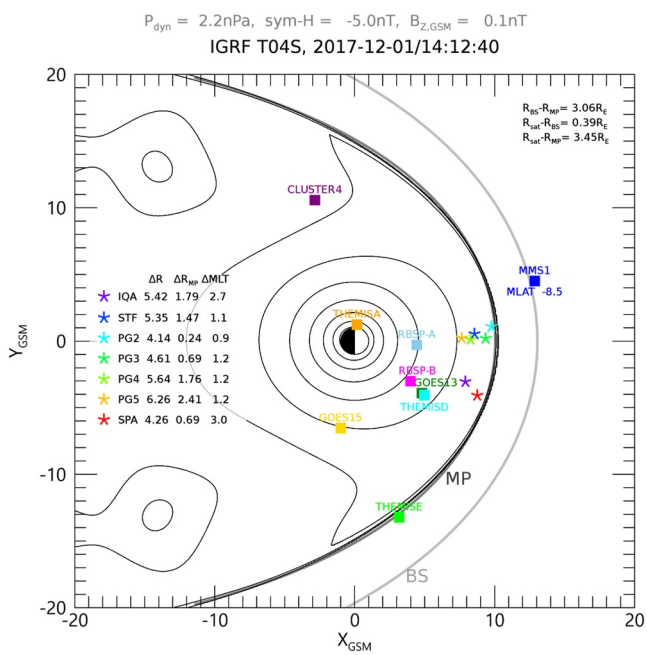

Figure 3. Top-down view of the equatorial magnetic field configuration at 14:12 UT obtained from the IGRF + TS05 magnetic field model. Star symbols indicate the location of the ground stations mapped to the magnetic equator. Square symbols indicate the location of various spacecraft.

and STF and PG stations were mostly about 1 hr, but IQA and SPA stations were about 3 hr separated from MMS. This means that the observed Pc1 waves were localized in their longitudinal extent as well and the source location was close to MMS.

The DC magnetic field observation showed a clear magnetic impulse event (MIE) at all stations slightly before the Pc1 waves were observed (~14:07). The MIEs were also observed in IQA and SPA stations several minutes after other stations. This indicates longitudinal (westward) propagation of MIEs. The traveling feature of the disturbances is more clearly seen in the spherical elementary currents estimated from ground magnetometers (Weygand et al., 2011) (Figure 5). The vortical current features started at 14:10 near the STF station (Figure 5b) and traveled westward over time in Figures 5c and 5d. Since a close relationship between FTs and MIEs has been reported by several papers (Fillingim et al., 2011; Jacobsen et al., 2009; Sibeck et al., 1999), we do not further discuss the observation of MIEs in this study. Note that longitudinal propagation is not present in the observed Pc1 waves.

3.3. Observation Time Difference Between the Hemispheres

In addition to the clear response time between FTs and ground features, there are observation time differences in Pc1 wave activity between the hemispheres. For simplicity of the comparison, we focus on events 1, 4, and 5 observed by STF (NH, $L = 8.85$) and PG4 (SH, $L = 8.59$) stations. Since the sensitivity of the sensors is different and not intercalibrated, we do not compare the onset time of the waves but rather use the cross-correlation of integrated power of frequency between 0.2 and 0.9 Hz to estimate the time difference. The results are shown in Table 2. Although the time differences varied by the events, all events were observed earlier in the northern hemisphere than in the southern hemisphere. Note that the time difference between peak power times and the delay time estimated from cross-correlation can be different but the trend that Pc1 waves were observed earlier in the northern hemisphere is still the same.

EMIC waves excited in the magnetosphere are often considered to propagate bi-directionally from the generation region (Loto'aniu et al., 2005) when the waves are excited by the anisotropic particle distribution. One possible source location of the wave activity can be found by radially extending down the location of FT events observed by MMS1 to the magnetopause. As the pressure impact propagates radially with the fast magnetosonic mode from its source region, the closest location on the magnetopause from the FT is the most probable region where the plasma would be intensely affected by the pressure change. For a more realistic estimation of the wave traveling time, we conducted an MHD simulation of our event to get the background plasma (density, temperature, and velocity) condition and magnetic field configuration using the University of Michigan Space Weather Modeling Framework (SWMF) Geospace Model configuration (Gombosi et al., 2021; Welling et al., 2021). The SWMF simulations were driven with propagated 1-min resolution OMNI data, using solar wind velocity (in km/s), density (in cm^{-3}), temperature (in K), and magnetic field vector (in nT). These values are used as upstream boundary conditions 32 R_E away from the Earth at the subsolar point. The simulations were first run on steady-state and then switched off. Time-accurate runs started at 11.00 UT using the OMNI data to allow for the system to reach a steady state before studying the observed phenomena. Note that the FT is related to the kinetic physics of ions. So, the MHD simulation does not incorporate the entire physical process from the formation of FT and

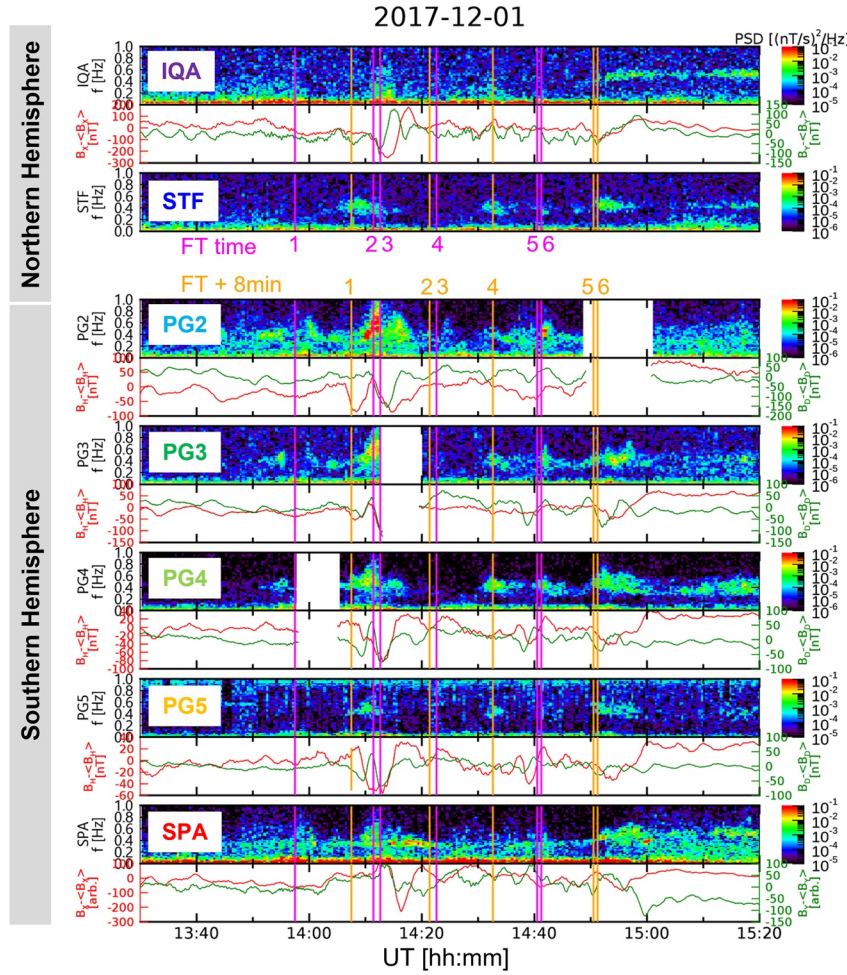

Figure 4. Spectrograms of the AC magnetic field (top panels) and horizontal components of the DC magnetic field measurement (bottom panels) from the northern hemispheric stations (IQA and STF) and the southern hemispheric stations (PG2, PG3, PG4, PG5, and SPA). The magenta lines in each panel indicate the event time of each foreshock transient (FT) event and the orange lines are 8 min after each FT event.

consequent wave generation but just provides global/background information near and in the Earth's magnetosphere. Considering the localized effect of FTs on the outside magnetosphere and our estimation depends heavily on the global scale plasma condition, however, the MHD simulation can be a good substitute for the global hybrid simulation which requires enormous computing resources.

Figure 6 shows the plasma density sliced in the meridional plane at MLT = 13.3 where MMS was located during the events. The magnetic field lines are traced in 3D space and then mapped to the plane. Assuming the pressure effect due to FT events is strongest at the closest location on the magnetopause, the possible impact location is located slightly below the magnetic equator ($Z_{SM} < 0$). This location is in the quasi-parallel bow shock region under the positive IMF X_{GSM} dominant with small negative IMF Z_{GSM} (see also Figure 2d). The cyan star indicates the location where the magnetic field line from the STF station crosses the radial line from MMS to the Earth, which could be considered as a source region of the wave. Thus, the traveling path of the wave along the magnetic field line is shorter toward the southern hemisphere than toward the northern hemisphere. This essentially indicates that the southern hemispheric stations should observe the wave activity earlier than the northern hemispheric stations unless the wave's propagation velocity is much faster in the northern hemisphere compared to the southern hemisphere. Our ground observations show the opposite trend. These observational results raise a question about bi-directional wave propagation. In order to explain the observed time difference between the hemispheres, we suggest that the possible wave generation region is not located at the impact region on the magnetopause but located at the two minimum B pockets which are represented by green stars in Figure 6.

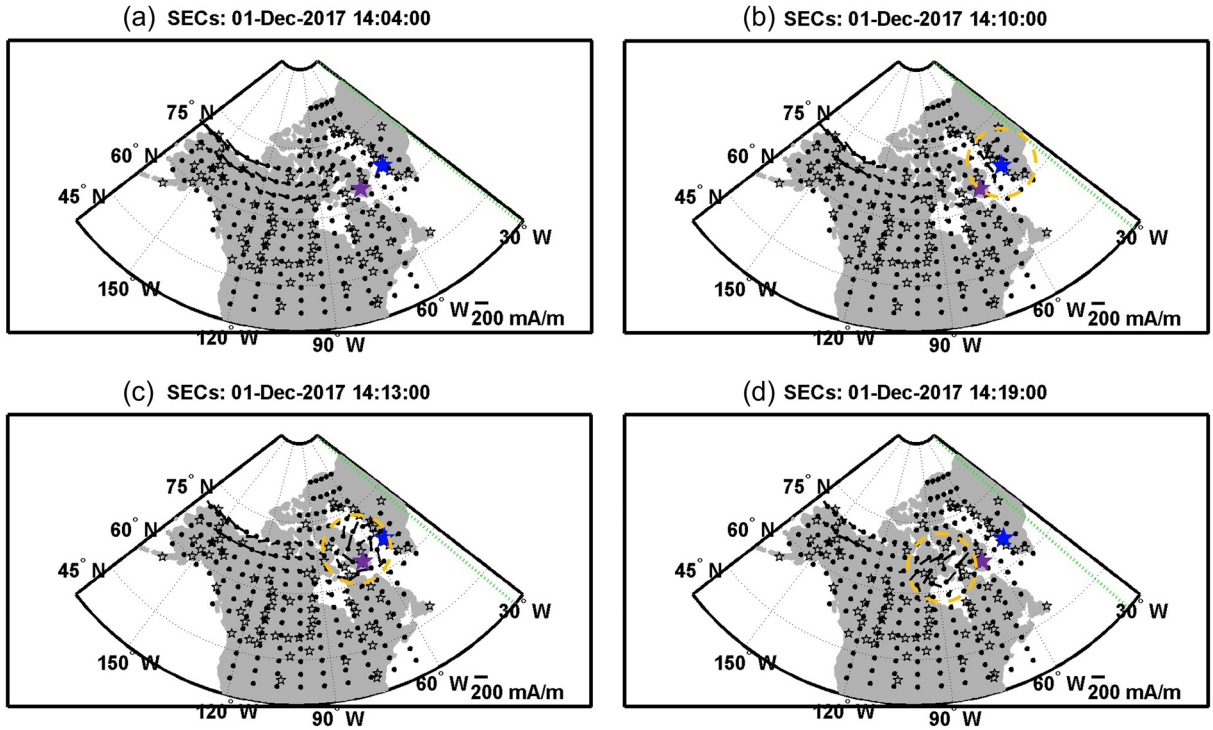

Figure 5. Spherical elementary current systems map of currents in the northern hemisphere for (a) 14:04, (b) 14:10, (c) 14:13, and (d) 14:19 during the foreshock transient events. The green dotted line indicates noon. STF (blue) and IQA (purple) stations are marked with star symbols. The orange dashed circles in (b–d) highlight magnetic impulse event signatures.

The minimum B pockets are determined by choosing the location where the magnetic field intensity is minimum in both hemispheres. Note that the magnetic field line in Figure 6a is projected from the 3D magnetic field line to the 2D plane (R and Z). The wave path from the minimum B pockets is shorter in the northern hemisphere than in the southern hemisphere. Therefore, waves can arrive on the ground in the northern hemisphere first then in the southern hemisphere.

We calculated the group velocity ($\boldsymbol{V_g} = \partial\boldsymbol{\omega}/\partial\boldsymbol{k}$, where ω is the angular frequency and k is the wave number) of a monotonic wave with $\boldsymbol{f/f_{cH^+} = 0.5}$, where $\boldsymbol{f_{cH^+}}$ is the proton gyrofrequency at the generation region, propagating along the field line. For the calculation, we used the plasma properties obtained from the MHD simulation result and assumed a proton-electron cold plasma dispersion relation for simplicity (Summers, 2005; Swanson, 1989).

$$\left(\frac{ck}{\omega}\right)^2 = 1 - \frac{\omega_{pe}^2}{\Omega_e^2}\frac{1+\frac{m_e}{m_p}}{\left(\frac{\omega}{|\Omega_e|}+1\right)\left(\frac{\omega}{|\Omega_e|}-\frac{m_e}{m_p}\right)}, \quad (1)$$

where c is the speed of light, ω_{pe} is the electron plasma frequency, $\mathbf{m_e}$ and $\mathbf{m_p}$ are the electron and proton mass, respectively.

Table 2
Peak Power Times of Pc1 Wave Events and Time Delays Estimated by Cross-Correlation for Events 1, 4, and 5 at STF and PG4 Stations

	Event 1	Event 4	Event 5
Wave peak at PG4	14:10:21	14:33:00	14:53:02
Wave peak at STF	14:08:35	14:31:37	14:52:05
Time delay between PG4 and STF from cross-correlation	76.8 s	25.8 s	51.0 s

Note. Please see the main text for the details of the time delay estimation.

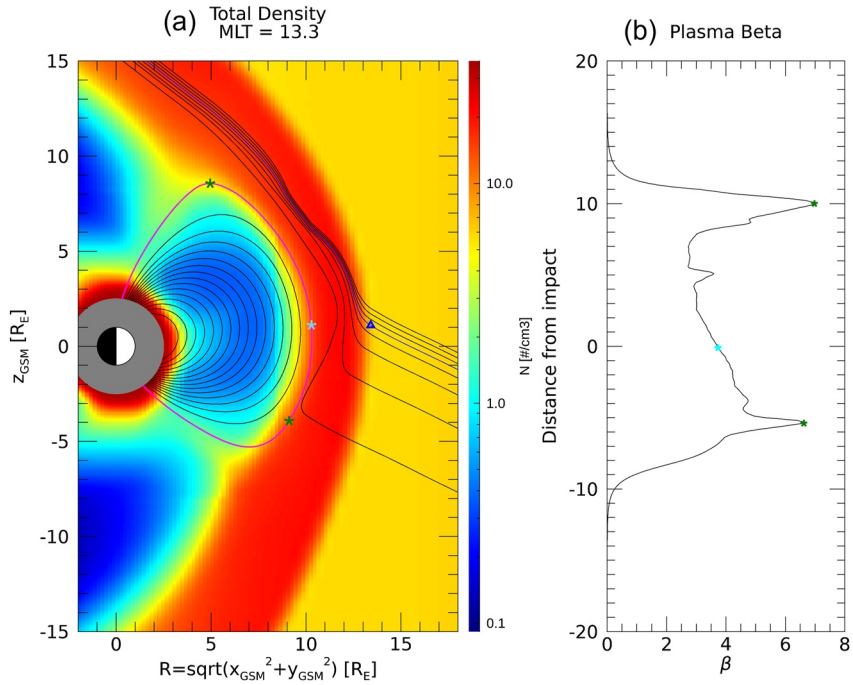

Figure 6. (a) Plasma density and magnetic field configuration and (b) plasma beta along the field line connected to STF station (magenta) obtained from MHD simulation at 14:00 UT. Blue triangle is the Magnetospheric Multiscale (MMS) location when foreshock transients are observed. Cyan star indicates the closest location to the field line from the MMS location. Green stars are the off-equatorial minimum B region on the magnetic field connected to the STF station.

Since the inner boundary of the MHD simulation is down to 2.5 R_E, we calculate the wave propagation time down to the inner boundary. The path length of the northward propagating wave along the field line from the northern hemispheric source region is ~8.0 R_E and the transit time is 104.5 s. The path length for the southward propagating wave from the southern hemispheric source region is ~9.5 R_E and the transit time is 186.4 s. Therefore, considering the wave excited at the off-equatorial minimum B pockets could be one possible mechanism for the FT-induced waves. In real space, of course, the plasma parameters may be different from the MHD simulation results. Therefore, the propagation velocity can be slightly different and the transit time difference between the hemispheres may vary. We discuss more details on the wave generation hypothesis in Section 4. Note also that the inclusion of heavier ions, such as He^+ and O^+, introduces a stopband, where the dispersion relation of the wave is not defined. Waves cannot propagate across the stopband without mode coupling and polarization reversal. Thus, the stopband makes the wave propagation complicated.

4. Summary and Discussion

In the present study, we reported a series of FT events observed by the MMS spacecraft and two types of ground signatures related to them, MIEs and Pc1 waves. MIEs were observed both in the northern and the southern hemispheres at the stations longitudinally close to the MMS location. Then the MIE traveled westward over time in both hemispheres. This longitudinal travel characteristic of MIE has been reported by several papers (Archer et al., 2015; Eastwood et al., 2008; Engebretson et al., 2013; H. Kim et al., 2017) as traveling convection vortices. The Pc1 wave observations from the array of ground magnetometers showed a systematic time difference of about 8 min between the FT events and ground responses in both hemispheres. The time difference is somewhat similar to the estimated time delay between a hot flow anomaly and a ground Pc3 wave observed by Eastwood et al. (2011).

There have been several studies that discuss the possible relationship between foreshock transients and ground Pc1 activities (Engebretson et al., 2013; Posch et al., 2013; Suvorova et al., 2019). Our study reports unique and clear observational characteristics which are distinct from previous studies.

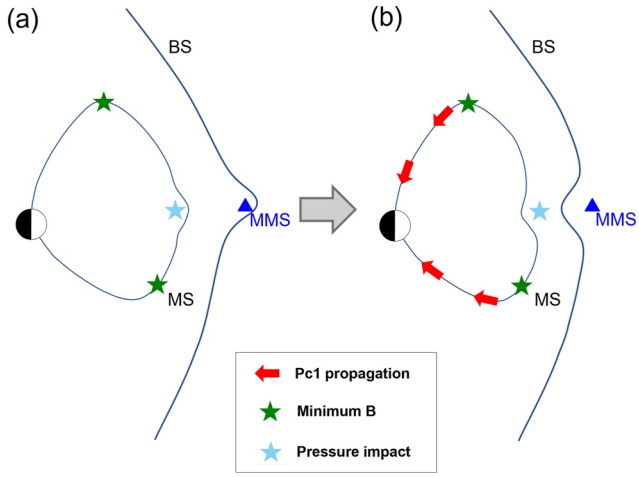

Figure 7. Schematics of wave propagation due to foreshock transients at (a) the outward motion and (b) the inward motion of the magnetopause.

1. We found that there were at least 3 events (events 1, 4, and 5 or 6) showing ~8 min time delay between space FT observations and ground Pc1 wave observations.
2. Waves were observed in both hemispheres in the high-latitude region.
3. During the entire event period, no inner magnetospheric EMIC waves were observed by spacecraft, such as Van Allen Probes, THEMIS, and GOES13 (Figure S1).
4. Wave observation times were slightly different between the hemispheres. Especially for STF and PG4 stations, waves were observed in the northern hemisphere first and then the southern hemisphere later.

The absence of Pc1 wave observation at SPA and IQA stations, longitudinally distant stations from the latitudinal array (PG and STF stations), indicates that these waves were longitudinally localized. The finite spatial structure of waves in the radial direction can be deduced from decreasing wave amplitude from PG2 to PG5. The overall observations indicate the Pc1 waves originated from the outer magnetosphere in a localized area.

The outer magnetospheric source region is supported by magnetospheric satellite observations. We have checked for wave activity using Van Allen Probes, THEMIS-D, and GOES13 data. These satellites are located inside the magnetosphere on the dayside (see Figure 3). None of them observed Pc1 waves during the event. Both Van Allen Probes and THEMIS-D showed lower frequency perturbations which might be a compressional mode produced by the fluctuation in the outer magnetosphere (Figure S1).

Our simultaneous observations of MIEs and Pc1 waves provide more information on the source region. While there is clear evidence that the MIE propagates westward, Pc1 waves are not observed (or very weak) in different longitudes at stations IQA and SPA. The MIE and Pc1 were probably triggered by the same FT at the same region where the impact was strongest, but the source of MIE latitudinally propagated through the surface wave (H. Zhang et al., 2022). On the other hand, the source of the Pc1 wave near the magnetopause is affected by pressure changes due to the impact of the FT in the upstream solar wind. The perturbation in the propagated region in the different longitudes is somehow not enough to excite Pc1 waves.

Here, we would like to elaborate on a possible scenario that can support the source region of the Pc1 waves in the off-equatorial minimum B pockets. Figure 7 shows a schematic of the propagation of the wave generated by FT events. First, the FT generates depletion of plasma pressure in the magnetosheath resulting in the outward motion of the magnetopause. The FT propagates the energy in other directions (could be longitudinally on the bow shock surface) so the bow shock and the magnetopause at the MMS longitude move inward due to the magnetic tension force. This out- and inward motion of the magnetopause could create the MIE event observed in the DC magnetic field. When the magnetopause moves inward, the minimum B pockets off the equator could be more distinct. Consequently, the plasmas at the minimum B region become anisotropic by the Shabansky orbit effect (McCollough et al., 2010) and then excite Pc1 (EMIC) waves. This scenario is based on the assumption that the waves are simultaneously excited at the off-equatorial minimum B pockets in both hemispheres. The simultaneous excitation of waves can be realized when the plasma condition is in the marginal state for the ion cyclotron instability; then the wave can be easily triggered by a small addition of free energy in the system. There have been several papers reporting magnetospheric plasmas are often in the marginal state for the ion cyclotron instability (Engebretson et al., 2018; Gary et al., 1994; Noh et al., 2018, 2021). This scenario is supported by the plasma beta estimated from the MHD simulation. Figure 6b shows the plasma beta distribution from the impact location (cyan star) along the magnetic field line indicated with the magenta curve in Figure 6a. It is well known that the ion cyclotron instability threshold condition has the inverse relationship between the temperature anisotropy and the plasma beta in which the anisotropy threshold for the instability gets lower in the high beta condition (Gary et al., 1976, 1994). The plasma betas at the minimum B pockets are high enough (>1) to consider the wave excitation. That means a small addition of anisotropy can make the plasma condition unstable to the ion cyclotron instability.

The reason for the absence of the ground wave observations corresponding to the FT events 2 and 3 is somewhat unclear. One possible explanation is the wave propagation effect. Propagation characteristics of EMIC waves

become more complicated when the waves are generated and propagated in the heavy ion plasma environment. In the cold plasma theory, the presence of heavy ions yields stopbands, thus waves cannot propagate across them without mode conversion, polarization reversal, or tunneling (E.-H. Kim & Johnson, 2016 and references therein). During the propagation, waves cannot penetrate the bi-ion frequency, where the polarization of the wave can be changed, thus they do not reach the ground. There is also high-frequency wave damping through ionospheric propagation (Fedorov et al., 2018; Noh et al., 2022). Noh et al. (2022) reported that ~54% of the waves observed in the geosynchronous orbit show coincident wave events on the ground at a magnetically connected ground station. On the other hand, E.-H. Kim and Johnson (2023) recently reported that EMIC waves started from high latitudes can easily propagate down to the ground since the efficiency of mode conversion during the propagation dramatically increases. Thus, without a conjugate observation at high latitude in the path of waves, the propagation effect cannot be confirmed.

Changes in the dispersion relation of waves may significantly affect the propagation characteristics. The ion outflow also can be different between the hemispheres due to different solar illumination, especially in summer and winter (M. J. Kim et al., 2023; Kitamura et al., 2021; Kronberg et al., 2014; Strangeway et al., 2005). The heavy ion content also can vary since the O^+ ions are more dependent on season than H+ ions (Glocer et al., 2020; Lennartsson et al., 2004). Therefore, a comprehensive modeling effort both in ion composition and wave propagation is necessary to study the interhemispheric wave propagation in the asymmetrically distributed ions between the hemispheres. This modeling effort is well beyond the scope of this paper which is an observational case study, and we leave this for future work.

Data Availability Statement

All search coil magnetometer data used in this study is available at http://mirl.unh.edu/ULF/cdf/ (Lessard, 2020). Fluxgate magnetometer data for all PG stations is available both at http://mist.ece.vt.edu/ and http://mist.nianet.org/CDFdata/ (R. Clauer et al., 2017). Fluxgate magnetometer data for SPA and IQA stations are available at https://antarcticgeospace.njit.edu/Data/ and https://imag-data.bgs.ac.uk/GIN_V1/GINForms2, respectively (Gerrard, 2017; INTERMAGNET, 2017). MMS burst mode data are available at https://lasp.colorado.edu/mms/sdc/public/datasets/ (Burch et al., 2015). Magnetometer data from Van Allen Probes, GOES13, and Themis-D, used in Figure S1 are available at https://cdaweb.gsfc.nasa.gov/pub/data/rbsp/, https://www.ncei.noaa.gov/data/goes-space-environment-monitor/access/science/mag/goes13/, and https://cdaweb.gsfc.nasa.gov/pub/data/themis/thd/l2/fgm/, respectively (Angelopoulos, 2021; Kletzing, 2022; Redmon, 2017). The SWFM simulation results are available at https://zenodo.org/record/8084912 (Noh, 2023).

Acknowledgments
We thank Natural Resource Canada (NRCan) for providing fluxgate magnetometer data from Iqaluit and facilitating the search-coil magnetometer at Iqaluit. This research was supported by the Los Alamos National Laboratory (LANL) through its Center for Space and Earth Science (CSES). CSES is funded by LANL's Laboratory Directed Research and Development (LDRD) program under Project 20210528CR. The work at New Jersey Institute of Technology was supported by NASA Grant 80NSSC21K0132, NSF Grants OPP-1744861, NSF-1602560, and AGS-2133837. The fluxgate magnetometer project at South Pole station is supported by NSF Grant OPP-1643700 to New Jersey Institute of Technology. JMW acknowledges NASA Contract 80GSFC17C0018, NASA Grants 80NSSC18K1220 and 80NSSC18K0570. MDH was supported by NSF AGS-2027210. The authors also acknowledge support by the International Space Science Institute (ISSI) in Bern, through the ISSI International Team project "Understanding Interhemispheric Asymmetry in MIT Coupling." We acknowledge use of NASA/GSFC's Space Physics Data Facility's OMNIWeb (or CDAWeb or ftp) service, and OMNI data. Resources supporting the simulation components of this work were provided by the NASA High-End Computing (HEC) Program through the NASA Advanced Supercomputing (NAS) Division at Ames Research Center.

References

Allen, R. C., Zhang, J.-C., Kistler, L. M., Spence, H. E., Lin, R.-L., Klecker, B., et al. (2015). A statistical study of EMIC waves observed by Cluster: 1. Wave properties. *Journal of Geophysical Research: Space Physics*, *120*(7), 5574–5592. https://doi.org/10.1002/2015JA021333

Anderson, B. J., Denton, R. E., Ho, G., Hamilton, D. C., Fuselier, S. A., & Strangeway, R. J. (1996). Observational test of local proton cyclotron instability in the Earth's magnetosphere. *Journal of Geophysical Research*, *101*(A10), 21527–21543. https://doi.org/10.1029/96JA01251

Anderson, B. J., Takahashi, K., Erlandson, R. E., & Zanetti, L. J. (1990). Pc1 pulsations observed by AMPTE/CCE in the Earth's outer magnetosphere. *Geophysical Research Letters*, *17*(11), 1853–1856. https://doi.org/10.1029/GL017i011p01853

Angelopoulos, V. (2021). THEMIS-D: Fluxgate magnetometer measurements 1/128s [Dataset]. Retrieved from https://spdf.gsfc.nasa.gov/pub/data/themis/thd/l2/fgm/

Archer, M. O., Turner, D. L., Eastwood, J. P., Horbury, T. S., & Schwartz, S. J. (2014). The role of pressure gradients in driving sunward magnetosheath flows and magnetopause motion. *Journal of Geophysical Research: Space Physics*, *119*(10), 8117–8125. https://doi.org/10.1002/2014JA020342

Archer, M. O., Turner, D. L., Eastwood, J. P., Schwartz, S. J., & Horbury, T. S. (2015). Global impacts of a Foreshock Bubble: Magnetosheath, magnetopause and ground-based observations. *Planetary and Space Science*, *106*, 56–66. https://doi.org/10.1016/j.pss.2014.11.026

Blum, L. W., Bonnell, J. W., Agapitov, O., Paulson, K., & Kletzing, C. (2017). EMIC wave scale size in the inner magnetosphere: Observations from the dual Van Allen Probes. *Geophysical Research Letters*, *44*(3), 1227–1233. https://doi.org/10.1002/2016GL072316

Blum, L. W., & Breneman, A. W. (2020). Observations of radiation belt losses due to cyclotron wave-particle interactions. In A. N. Jaynes & M. E. Usanova (Eds.), *The dynamic loss of Earth's radiation belts* (pp. 49–98). Elsevier. https://doi.org/10.1016/B978-0-12-813371-2.00003-2

Blum, L. W., Halford, A., Millan, R., Bonnell, J. W., Goldstein, J., Usanova, M., et al. (2015). Observations of coincident EMIC wave activity and duskside energetic electron precipitation on 18-19 January 2013. *Geophysical Research Letters*, *42*(14), 5727–5735. https://doi.org/10.1002/2015GL065245

Burch, J. L., Fowler, G., & Le, G. (2015). MMS Science data center [Dataset]. Retrieved from https://lasp.colorado.edu/mms/sdc/public/datasets/

Burch, J. L., Moore, T. E., Torbert, R. B., & Giles, B. L. (2016). Magnetospheric multiscale overview and science objectives. *Space Science Reviews*, *199*(1–4), 5–21. https://doi.org/10.1007/s11214-015-0164-9

Capannolo, L., Li, W., Ma, Q., Chen, L., Shen, X. C., Spence, H. E., et al. (2019). Direct observation of subrelativistic electron precipitation potentially driven by EMIC waves. *Geophysical Research Letters*, *46*(22), 12711–12721. https://doi.org/10.1029/2019GL084202

Cho, J.-H., Lee, D.-Y., Noh, S.-J., Kim, H., Choi, C. R., Lee, J., & Hwang, J. (2017). Spatial dependence of electromagnetic ion cyclotron waves triggered by solar wind dynamic pressure enhancements. *Journal of Geophysical Research: Space Physics*, *122*(5), 5502–5518. https://doi.org/10.1002/2016JA023827

Cho, J.-H., Lee, D.-Y., Noh, S.-J., Shin, D.-K., Hwang, J., Kim, K.-C., et al. (2016). Van Allen Probes observations of electromagnetic ion cyclotron waves triggered by enhanced solar wind dynamic pressure. *Journal of Geophysical Research: Space Physics*, *121*(10), 9771–9793. https://doi.org/10.1002/2016JA022841

Clauer, C. R., Kim, H., Deshpande, K., Xu, Z., Weimer, D., Musko, S., et al. (2014). An autonomous adaptive low-power instrument platform (AAL-PIP) for remote high-latitude geospace data collection. *Geoscientific Instrumentation, Methods and Data Systems*, *3*(2), 211–227. https://doi.org/10.5194/gi-3-211-2014

Clauer, R., Xu, Z., Weimer, D. R., Hartinger, M., Kim, H., Coyle, S., et al. (2017). Virginia tech MIST [Dataset]. Retrieved from http://mist.ece.vt.edu/downloads

Clausen, L. B. N., Baker, J. B. H., Ruohoniemi, J. M., & Singer, H. J. (2011). EMIC waves observed at geosynchronous orbit during solar minimum: Statistics and excitation. *Journal of Geophysical Research*, *116*(A10), A10205. https://doi.org/10.1029/2011JA016823

Cornwall, J. M., Coroniti, F. V., & Thorne, R. M. (1970). Turbulent loss of ring current protons. *Journal of Geophysical Research*, *75*(25), 4699–4709. https://doi.org/10.1029/JA075i025p04699

Eastwood, J. P., Schwartz, S. J., Horbury, T. S., Carr, C. M., Glassmeier, K.-H., Richter, I., et al. (2011). Transient Pc3 wave activity generated by a hot flow anomaly: Cluster, Rosetta, and ground-based observations. *Journal of Geophysical Research*, *116*(A8), A08224. https://doi.org/10.1029/2011JA016467

Eastwood, J. P., Sibeck, D. G., Angelopoulos, V., Phan, T. D., Bale, S. D., McFadden, J. P., et al. (2008). THEMIS observations of a hot flow anomaly: Solar wind, magnetosheath, and ground-based measurements. *Geophysical Research Letters*, *35*(17), L17S03. https://doi.org/10.1029/2008GL033475

Engebretson, M. J., Posch, J. L., Capman, N. S. S., Campuzano, N. G., Bělik, P., Allen, R. C., et al. (2018). MMS, Van Allen Probes, GOES 13, and ground-based magnetometer observations of EMIC wave events before, during, and after a modest interplanetary shock. *Journal of Geophysical Research: Space Physics*, *123*(10), 8331–8357. https://doi.org/10.1029/2018JA025984

Engebretson, M. J., Yeoman, T. K., Oksavik, K., Søraas, F., Sigernes, F., Moen, J. I., et al. (2013). Multi-instrument observations from Svalbard of a traveling convection vortex, electromagnetic ion cyclotron wave burst, and proton precipitation associated with a bow shock instability. *Journal of Geophysical Research: Space Physics*, *118*(6), 2975–2997. https://doi.org/10.1002/jgra.50291

Fedorov, E. N., Pilipenko, V. A., Engebretson, M. J., & Hartinger, M. D. (2018). Transmission of a magnetospheric Pc1 wave beam through the ionosphere to the ground. *Journal of Geophysical Research: Space Physics*, *123*(5), 3965–3982. https://doi.org/10.1029/2018JA025338

Fillingim, M. O., Eastwood, J., Parks, G., Angelopoulos, V., Mann, I., Mende, S., & Weatherwax, A. (2011). Polar UVI and THEMIS GMAG observations of the ionospheric response to a hot flow anomaly. *Journal of Atmospheric and Solar-Terrestrial Physics*, *73*(1), 137–145. https://doi.org/10.1016/j.jastp.2010.03.001

Fraser, B. J., & McPherron, R. L. (1982). Pc 1-2 magnetic pulsation spectra and heavy ion effects at synchronous orbit: ATS 6 results. *Journal of Geophysical Research*, *87*(A6), 4560–4566. https://doi.org/10.1029/JA087iA06p04560

Gary, S. P., Moldwin, M. B., Thomsen, M. F., Winske, D., & McComas, D. J. (1994). Hot proton anisotropies and cool proton temperatures in the outer magnetosphere. *Journal of Geophysical Research*, *99*(A12), 23603–23615. https://doi.org/10.1029/94JA02069

Gary, S. P., Montgomery, M. D., Feldman, W. C., & Forslund, D. W. (1976). Proton temperature anisotropy instabilities in the solar wind. *Journal of Geophysical Research*, *81*(7), 1241–1246. https://doi.org/10.1029/ja081i007p01241

Gerrard, A. (2017). Antarctic Geospace data portal [Dataset]. Retrieved from https://antarcticgeospace.njit.edu/Data/

Glocer, A., Welling, D., Chappell, C. R., Toth, G., Fok, M.-C., Komar, C., et al. (2020). A case study on the origin of near-Earth plasma. *Journal of Geophysical Research: Space Physics*, *125*(11), e2020JA028205. https://doi.org/10.1029/2020JA028205

Gombosi, T. I., Chen, Y., Glocer, A., Huang, Z., Jia, X., Liemohn, M. W., et al. (2021). What sustained multi-disciplinary research can achieve: The space weather modeling framework. *Journal of Space Weather and Space Climate*, *11*, 42. https://doi.org/10.1051/swsc/2021020

Halford, A. J., Fraser, B. J., & Morley, S. K. (2010). EMIC wave activity during geomagnetic storm and nonstorm periods: CRRES results. *Journal of Geophysical Research*, *115*(A12), A12248. https://doi.org/10.1029/2010JA015716

Hartinger, M. D., Turner, D. L., Plaschke, F., Angelopoulos, V., & Singer, H. (2013). The role of transient ion foreshock phenomena in driving Pc5 ULF wave activity. *Journal of Geophysical Research: Space Physics*, *118*(1), 299–312. https://doi.org/10.1029/2012JA018349

INTERMAGNET. (2017). INTERMAGNET - British geological survey [Dataset]. Retrieved from https://imag-data.bgs.ac.uk/GIN_V1/GINForms2

Jacobsen, K. S., Phan, T. D., Eastwood, J. P., Sibeck, D. G., Moen, J. I., Angelopoulos, V., et al. (2009). THEMIS observations of extreme magnetopause motion caused by a hot flow anomaly. *Journal of Geophysical Research*, *114*(A8), A08210. https://doi.org/10.1029/2008JA013873

Jordanova, V. K., Albert, J., & Miyoshi, Y. (2008). Relativistic electron precipitation by EMIC waves from self-consistent global simulations. *Journal of Geophysical Research*, *113*(A3), A00A10. https://doi.org/10.1029/2008JA013239

Jun, C. W., Yue, C., Bortnik, J., Lyons, L. R., Nishimura, Y., & Kletzing, C. (2019). EMIC wave properties associated with and without injections in the inner magnetosphere. *Journal of Geophysical Research: Space Physics*, *124*(3), 2029–2045. https://doi.org/10.1029/2018JA026279

Keika, K., Takahashi, K., Ukhorskiy, A. Y., & Miyoshi, Y. (2013). Global characteristics of electromagnetic ion cyclotron waves: Occurrence rate and its storm dependence. *Journal of Geophysical Research: Space Physics*, *118*(7), 4135–4150. https://doi.org/10.1002/jgra.50385

Kennel, C. F., & Petschek, H. E. (1966). Limit on stably trapped particle fluxes. *Journal of Geophysical Research*, *71*(1), 1–28. https://doi.org/10.1029/JZ071i001p00001

Kim, E.-H., & Johnson, J. R. (2016). Full-wave modeling of EMIC waves near the He+ gyrofrequency. *Geophysical Research Letters*, *43*(1), 13–21. https://doi.org/10.1002/2015GL066978

Kim, E.-H., & Johnson, J. R. (2023). Magnetic tilt effect on externally driven electromagnetic ion cyclotron (EMIC) waves. *Geophysical Research Letters*, *50*(6), e2022GL101544. https://doi.org/10.1029/2022GL101544

Kim, H., Lessard, M. R., Jones, S. L., Lynch, K. A., Fernandes, P. A., Aruliah, A. L., et al. (2017). Simultaneous observations of traveling convection vortices: Ionosphere-thermosphere coupling. *Journal of Geophysical Research: Space Physics*, *122*(5), 4943–4959. https://doi.org/10.1002/2017JA023904

Kim, H., Schiller, Q., Engebretson, M. J., Noh, S., Kuzichev, I., Lanzerotti, L. J., et al. (2021). Observations of particle loss due to injection-associated electromagnetic ion cyclotron waves. *Journal of Geophysical Research: Space Physics*, *126*(2), e2020JA028503. https://doi.org/10.1029/2020JA028503

Kim, M. J., Goldstein, J., Fuselier, S. A., Glocer, A., & Burch, J. L. (2023). A multi-satellite case study of low-energy H+ asymmetric field-aligned distributions observed by MMS in the Earth's magnetosphere. *Journal of Geophysical Research: Space Physics*, *128*(3), e2022JA031060. https://doi.org/10.1029/2022JA031060

Kitamura, N., Seki, K., Keika, K., Nishimura, Y., Hori, T., Hirahara, M., et al. (2021). On the relationship between energy input to the ionosphere and the ion outflow flux under different solar zenith angles. *Earth Planets and Space*, *73*(1), 202. https://doi.org/10.1186/s40623-021-01532-y

Kletzing, C. (2022). Van Allen Probe A fluxgate magnetometer high resolution data in GSM coordinates [Dataset]. https://doi.org/10.48322/2tyy-s986

Kronberg, E. A., Ashour-Abdalla, M., Dandouras, I., Delcourt, D. C., Grigorenko, E. E., Kistler, L. M., et al. (2014). Circulation of heavy ions and their dynamical effects in the magnetosphere: Recent observations and models. *Space Science Reviews*, *184*(1–4), 173–235. https://doi.org/10.1007/s11214-014-0104-0

Lanzerotti, L. J., Wolfe, A., Trivedi, N., Maclennan, C. G., & Medford, L. V. (1990). Magnetic impulse events at high latitudes: Magnetopause and boundary layer plasma processes. *Journal of Geophysical Research*, *95*(A1), 97–107. https://doi.org/10.1029/JA095iA01p00097

Lee, D.-Y. (2021). Sensitive dependence of ultrarelativistic electron precipitation on EMIC wave frequency. *Journal of Geophysical Research: Space Physics*, *126*(3), e2020JA028270. https://doi.org/10.1029/2020JA028270

Lee, J., Min, K., & Kim, K.-S. (2013). Characteristic dimension of electromagnetic ion cyclotron wave activity in the magnetosphere. *Journal of Geophysical Research: Space Physics*, *118*(4), 1651–1658. https://doi.org/10.1002/jgra.50242

Lennartsson, O. W., Collin, H. L., & Peterson, W. K. (2004). Solar wind control of Earth's H+ and O+ outflow rates in the 15-eV to 33-keV energy range. *Journal of Geophysical Research*, *109*(A12), A12212. https://doi.org/10.1029/2004JA010690

Lessard, M. (2020). Magnetosphere-Ionosphere Research Lab [Dataset]. Retrieved from http://mirl.unh.edu/ULF/cdf/

Lin, Y. (1997). Generation of anomalous flows near the bow shock by its interaction with interplanetary discontinuities. *Journal of Geophysical Research*, *102*(A11), 24265–24281. https://doi.org/10.1029/97JA01989

Lin, Y. (2002). Global hybrid simulation of hot flow anomalies near the bow shock and in the magnetosheath. *Planetary and Space Science*, *50*(5–6), 577–591. https://doi.org/10.1016/s0032-0633(02)00037-5

Liu, Y. H., Fraser, B. J., Menk, F. W., Zhang, J.-C., Kistler, L. M., & Dandouras, I. (2013). Correction to "Pc2 EMIC waves generated high off the equator in the dayside outer magnetosphere". *Geophysical Research Letters*, *40*(10), 1950–1951. https://doi.org/10.1002/grl.50283

Loto'aniu, T. M., Fraser, B. J., & Waters, C. L. (2005). Propagation of electromagnetic ion cyclotron wave energy in the magnetosphere. *Journal of Geophysical Research*, *110*(A7), A07214. https://doi.org/10.1029/2004JA010816

McCollough, J. P., Elkington, S. R., Usanova, M. E., Mann, I. R., Baker, D. N., & Kale, Z. C. (2010). Physical mechanisms of compressional EMIC wave growth. *Journal of Geophysical Research*, *115*(A10), A10214. https://doi.org/10.1029/2010JA015393

Meredith, N. P., Thorne, R. M., Horne, R. B., Summers, D., Fraser, B. J., & Anderson, R. R. (2003). Statistical analysis of relativistic electron energies for cyclotron resonance with EMIC waves observed on CRRES. *Journal of Geophysical Research*, *108*(A6), 1250. https://doi.org/10.1029/2002JA009700

Newell, P. T., & Gjerloev, J. W. (2011). Evaluation of SuperMAG auroral electrojet indices as indicators of substorms and auroral power. *Journal of Geophysical Research*, *116*(A12), A12211. https://doi.org/10.1029/2011JA016779

Newell, P. T., & Gjerloev, J. W. (2012). SuperMAG-based partial ring current indices. *Journal of Geophysical Research*, *117*(A5). https://doi.org/10.1029/2012JA017586

Ni, B., Cao, X., Zou, Z., Zhou, C., Gu, X., Bortnik, J., et al. (2015). Resonant scattering of outer zone relativistic electrons by multiband EMIC waves and resultant electron loss time scales. *Journal of Geophysical Research: Space Physics*, *120*(9), 7357–7373. https://doi.org/10.1002/2015JA021466

Noh, S.-J. (2023). Dataset for "Interhemispheric propagation of ULF waves caused by foreshock transients under quiet solar wind conditions" [Dataset]. Zenodo. https://doi.org/10.5281/zenodo.8084912

Noh, S.-J., Kim, H., Lessard, M., Engebretson, M., Pilipenko, V., Kim, E.-H., et al. (2022). Statistical study of EMIC wave propagation using space-ground conjugate observations. *Journal of Geophysical Research: Space Physics*, *127*(7), e2022JA030262. https://doi.org/10.1029/2022JA030262

Noh, S.-J., Lee, D.-Y., Choi, C.-R., Kim, H., & Skoug, R. (2018). Test of ion cyclotron resonance instability using proton distributions obtained from Van Allen Probe-A observations. *Journal of Geophysical Research: Space Physics*, *123*(8), 6591–6610. https://doi.org/10.1029/2018JA025385

Noh, S.-J., Lee, D.-Y., Kim, H., Lanzerotti, L. J., Gerrard, A., & Skoug, R. M. (2021). Upper limit of proton anisotropy and its relation to electromagnetic ion cyclotron waves in the inner magnetosphere. *Journal of Geophysical Research: Space Physics*, *126*(5), e2020JA028614. https://doi.org/10.1029/2020JA028614

Omidi, N., Berchem, J., Sibeck, D., & Zhang, H. (2016). Impacts of spontaneous hot flow anomalies on the magnetosheath and magnetopause. *Journal of Geophysical Research: Space Physics*, *121*(4), 3155–3169. https://doi.org/10.1002/2015JA022170

Omidi, N., Eastwood, J. P., & Sibeck, D. G. (2010). Foreshock bubbles and their global magnetospheric impacts. *Journal of Geophysical Research*, *115*(A6), A06204. https://doi.org/10.1029/2009JA014828

Omidi, N., & Sibeck, D. G. (2007). Formation of hot flow anomalies and solitary shocks. *Journal of Geophysical Research*, *112*(A1), A10203. https://doi.org/10.1029/2006JA011663

Papitashvili, N. E., & King, J. H. (2020). *"OMNI 1-min Data" Solar wind dynamic pressure and interplanetary magnetic field in GSM coordinate system*. NASA Space Physics Data Facility. https://doi.org/10.48322/45bb-8792

Pollock, C. T., Moore, A., Jacques, A., Burch, J., Gliese, U., Saito, Y., et al. (2016). Fast plasma investigation for magnetospheric multiscale. *Space Science Reviews*, *199*(1–4), 331–406. https://doi.org/10.1007/s11214-016-0245-4

Posch, J. L., Engebretson, M. J., Witte, A. J., Murr, D. L., Lessard, M. R., Johnsen, M. G., et al. (2013). Simultaneous traveling convection vortex events and Pc1 wave bursts at cusp latitudes observed in Arctic Canada and Svalbard. *Journal of Geophysical Research: Space Physics*, *118*(10), 6352–6363. https://doi.org/10.1002/jgra.50604

Redmon, R. (2017). NOAA National Centers for Environmental Information (GOES 13) [Dataset]. Retrieved from https://www.ncei.noaa.gov/data/goes-space-environment-monitor/access/science/mag/goes13/

Remya, B., Sibeck, D. G., Halford, A. J., Murphy, K. R., Reeves, G. D., Singer, H. J., et al. (2018). Ion injection triggered EMIC waves in the Earth's magnetosphere. *Journal of Geophysical Research: Space Physics*, *123*(6), 4921–4938. https://doi.org/10.1029/2018JA025354

Russell, C. T., Anderson, B. J., Baumjohann, W., Bromund, K. R., Dearborn, D., Fischer, D., et al. (2016). The magnetospheric multiscale magnetometers. *Space Science Reviews*, *199*(1–4), 189–256. https://doi.org/10.1007/s11214-014-0057-3

Schwartz, S. J., Chaloner, C. P., Christiansen, P. J., Coates, A. J., Hall, D. S., Johnstone, A. D., et al. (1985). An active current sheet in the solar wind. *Nature*, *318*(6043), 269–271. https://doi.org/10.1038/318269a0

Shi, F., Lin, Y., Wang, X., Wang, B., & Nishimura, Y. (2021). 3-D global hybrid simulations of magnetospheric response to foreshock processes. *Earth Planets and Space*, *73*(1), 138. https://doi.org/10.1186/s40623-021-01469-2

Sibeck, D. G., Borodkova, N. L., Schwartz, S. J., Owen, C. J., Kessel, R., Kokubun, S., et al. (1999). Comprehensive study of the magnetospheric response to a hot flow anomaly. *Journal of Geophysical Research*, *104*(A3), 4577–4593. https://doi.org/10.1029/1998JA900021

Strangeway, R. J., Ergun, R. E., Su, Y.-J., Carlson, C. W., & Elphic, R. C. (2005). Factors controlling ionospheric outflows as observed at intermediate altitudes. *Journal of Geophysical Research*, *110*(A3), A03221. https://doi.org/10.1029/2004JA010829

Summers, D. (2005). Quasi-linear diffusion coefficients for field-aligned electromagnetic waves with applications to the magnetosphere. *Journal of Geophysical Research*, *110*(A8), A08213. https://doi.org/10.1029/2005JA011159

Summers, D., & Thorne, R. M. (2003). Relativistic electron pitch-angle scattering by electromagnetic ion cyclotron waves during geomagnetic storms. *Journal of Geophysical Research*, *108*(A4), 1143. https://doi.org/10.1029/2002JA009489

Suvorova, A. V., Dmitriev, A. V., Parkhomov, V. A., & Tsegmed, B. (2019). Quiet time structured Pc1 waves generated during transient foreshock. *Journal of Geophysical Research: Space Physics*, *124*(11), 9075–9093. https://doi.org/10.1029/2019JA026936

Swanson, D. G. (1989). *Plasma waves*. Academic, Elsevier.

Thébault, E., Finlay, C. C., Beggan, C. D., Alken, P., Aubert, J., Barrois, O., et al. (2015). International geomagnetic reference field: The 12th generation. *Earth Planets and Space*, *67*(1), 79. https://doi.org/10.1186/s40623-015-0228-9

Thorne, R. M., Horne, R. B., Jordanova, V. K., Bortnik, J., & Glauert, S. (2006). Interaction of Emic waves with thermal plasma and radiation belt particles. In K. Takahashi, P. J. Chi, R. E. Denton, & R. L. Lysak (Eds.), *Magnetospheric ULF waves: Synthesis and New directions* (pp. 213–223). American Geophysical Union. https://doi.org/10.1029/169GM14

Thorne, R. M., & Kennel, C. F. (1971). Relativistic electron precipitation during magnetic storm main phase. *Journal of Geophysical Research*, *76*(19), 4446–4453. https://doi.org/10.1029/JA076i019p04446

Torbert, R. B., Russell, C. T., Magnes, W., Ergun, R. E., Lindqvist, P. A., LeContel, O., et al. (2016). The FIELDS instrument suite on MMS: Scientific objectives, measurements, and data products. *Space Science Reviews*, *199*(1–4), 105–135. https://doi.org/10.1007/s11214-014-0109-8

Tsyganenko, N. A., & Sitnov, M. I. (2005). Modeling the dynamics of the inner magnetosphere during strong geomagnetic storms. *Journal of Geophysical Research*, *110*(A3), A03208. https://doi.org/10.1029/2004JA010798

Turner, D. L., Liu, T. Z., Wilson, L. B., III, Cohen, I. J., Gershman, D. G., Fennell, J. F., et al. (2020). Microscopic, multipoint characterization of foreshock bubbles with Magnetospheric Multiscale (MMS). *Journal of Geophysical Research: Space Physics*, *125*(7), e2019JA027707. https://doi.org/10.1029/2019JA027707

Turner, D. L., Omidi, N., Sibeck, D. G., & Angelopoulos, V. (2013). First observations of foreshock bubbles upstream of Earth's bow shock: Characteristics and comparisons to HFAs. *Journal of Geophysical Research: Space Physics*, *118*(4), 1552–1570. https://doi.org/10.1002/jgra.50198

Usanova, M. E. (2021). Energy exchange between electromagnetic ion cyclotron (EMIC) waves and thermal plasma: From theory to observations. *Frontiers in Astronomy and Space Sciences*, *8*, 744344. https://doi.org/10.3389/fspas.2021.744344

Usanova, M. E., Mann, I. R., Bortnik, J., Shao, L., & Angelopoulos, V. (2012). THEMIS observations of electromagnetic ion cyclotron wave occurrence: Dependence on AE, SYMH, and solar wind dynamic pressure. *Journal of Geophysical Research*, *117*(A10), A10218. https://doi.org/10.1029/2012JA018049

Usanova, M. E., Mann, I. R., Kale, Z. C., Rae, I. J., Sydora, R. D., Sandanger, M., et al. (2010). Conjugate ground and multisatellite observations of compression-related EMIC Pc1 waves and associated proton precipitation. *Journal of Geophysical Research*, *115*(A7), A07208. https://doi.org/10.1029/2009JA014935

Vines, S. K., Allen, R. C., Anderson, B. J., Engebretson, M. J., Fuselier, S. A., Russell, C. T., et al. (2019). EMIC waves in the outer magnetosphere: Observations of an off-equator source region. *Geophysical Research Letters*, *46*(11), 5707–5716. https://doi.org/10.1029/2019GL082152

Wang, B., Liu, T., Nishimura, Y., Zhang, H., Hartinger, M., Shi, X., et al. (2020). Global propagation of magnetospheric Pc5 ULF waves driven by foreshock transients. *Journal of Geophysical Research: Space Physics*, *125*(12), e2020JA028411. https://doi.org/10.1029/2020JA028411

Wang, B., Zhang, H., Liu, Z., Liu, T., Li, X., & Angelopoulos, V. (2021). Energy modulations of magnetospheric ions induced by foreshock transient-driven ultralow-frequency waves. *Geophysical Research Letters*, *48*(10), e2021GL093913. https://doi.org/10.1029/2021GL093913

Wang, C.-P., Wang, X., Liu, T. Z., & Lin, Y. (2021). Impact of foreshock transients on the flank magnetopause and magnetosphere and the ionosphere. *Frontiers in Astronomy and Space Sciences*, *8*, 751244. https://doi.org/10.3389/fspas.2021.751244

Welling, D. T., Love, J. J., Rigler, E. J., Oliveira, D. M., Komar, C. M., & Morley, S. K. (2021). Numerical simulations of the geospace response to the arrival of an idealized perfect interplanetary coronal mass ejection. *Space Weather*, *19*(2), e2020SW002489. https://doi.org/10.1029/2020SW002489

Weygand, J. M., Amm, O., Viljanen, A., Angelopoulos, V., Murr, D., Engebretson, M. J., et al. (2011). Application and validation of the spherical elementary currents systems technique for deriving ionospheric equivalent currents with the North American and Greenland ground magnetometer arrays. *Journal of Geophysical Research*, *116*(A3), A03305. https://doi.org/10.1029/2010JA016177

Xue, Z., Yuan, Z., Yu, X., Deng, D., Huang, Z., & Raita, T. (2022). EMIC waves observed throughout the inner magnetosphere driven by abrupt enhancement of the solar wind pressure. *Geophysical Research Letters*, *49*(9), e2022GL098954. https://doi.org/10.1029/2022GL098954

Yahnin, A. G., Popova, T. A., Demekhov, A. G., Lubchich, A. A., Matsuoka, A., Asamura, K., et al. (2021). Evening side EMIC waves and related proton precipitation induced by a substorm. *Journal of Geophysical Research: Space Physics*, *126*(7), e29091. https://doi.org/10.1029/2020JA029091

Zhang, H., Zong, Q., Connor, H., Delamere, P., Facskó, G., Han, D., et al. (2022). Dayside transient phenomena and their impact on the magnetosphere and ionosphere. *Space Science Reviews*, *218*, 5. https://doi.org/10.1007/s11214-021-00865-0

Zhang, X. J., Mourenas, D., Artemyev, A. V., Angelopoulos, V., & Sauvaud, J. A. (2019). Precipitation of MeV and sub-MeV electrons due to combined effects of EMIC and ULF waves. *Journal of Geophysical Research: Space Physics*, *124*(10), 7923–7935. https://doi.org/10.1029/2019JA026566